PCCP

Accepted Manuscript

ROYAL SOCIETY OF CHEMISTRY

www.rsc.org/pccp

PCCP

RSCPublishing

PERSPECTIVES ARTICLE

Dielectric Function of Two-Phase Colloid-Polymer Nanocomposite

S.Mitzscherling,[a] Q. Cui[a], W.Koopman,[a*] and M. Bargheer[ab],

Cite this: DOI: 10.1039/xoxxooooox

Received ooth January 2012,
Accepted ooth January 2012

DOI: 10.1039/xoxxooooox

www.rsc.org/

The plasmon resonance of metal nanoparticles determines their optical response in the visible spectral range. Many details such as the electronic properties of gold near the particle surface and the local environment of the particles influence the spectra. We show how the cheap but highly precise fabrication of composite nanolayers by spin-assisted layer-by-layer deposition of polyelectrolytes can be used to investigate the spectral response of gold nanospheres (GNS) and gold nanorods (GNR) in a self-consistent way, using the established Maxwell-Garnett effective medium (MGEM) theory beyond the limit of homogeneous media. We show that the dielectric function of gold nanoparticles differs from the bulk value and experimentally characterize the shape and the surrounding of the particles thoroughly by SEM, AFM and ellipsometry. Averaging the dielectric functions of the layered surrounding by an appropriate weighting with the electric field intensity yields excellent agreement for the spectra of several nanoparticles and nanorods with various cover-layer thicknesses.

Introduction

Nanocomposite materials consisting of noble-metal colloids in polymer matrices have a huge potential for applications as surface coatings [1–3], for biomedical devices as implants[4,5] or drug delivery[6,7], and in optoelectronic devices[8,9]. The collective excitation of electrons at the colloid-surface determines the characteristic (optical) properties of these materials[10,11]. These localized surface Plasmons (LSPs) have been subject to extended theoretical modelling[10–15] and experimental investigations[10,11,16–22]. Studies have e.g. investigated the influence of surface modifications[22], and of the embedding media[10,23] on the LSP properties. In particular the sensitivity of the LSP to the dielectric properties of the environment is highly relevant for applications, like the fabrication of extremely precise sensors [24–27]

Layer-by-layer (LbL) deposition is an increasingly popular technique for the directed assembly of high quality polymer thin-films with colloid inclusions[16,22]. It provides an ultra-low cost fabrication technique for forming highly robust composites based on the electrostatic interaction of polyelectrolyte polymers[12]. Unlike conventional nanocomposites these LbL-films are highly homogenous and allow a very precise control of the layer-thickness[12,13]. These films are therefore an ideal candidate for the fabrication of low-cost high quality nanocomposites.

Effective medium theories, like the *Maxwell-Garnett Effective Medium* (MGEM) describe the dielectric-function of plasmonic nanocomposites[10,28–30]. Strictly speaking, the applicability of MGEM is confined to inclusions in a homogeneous matrix materials. In case of ultra-thin LbL-films where the thickness of the polymer matrix is in the range of the size of the metal inclusions, this assumption might not be fulfilled. As in this case the plasmon excitation extends outside the film, the dielectric surrounding effectively consists of two phases: the polymer matrix and the outside environment. For a correct prediction of the plasmon behavior in these materials, elaborated numerical simulations are commonly used even for simple particle geometries[14,15,31,32] However, in many situations, a fast procedure to approximate the plasmon resonance of these films would be of great advantage.

This perspectives article presents an LbL fabrication technique for preparing nanocomposite films and discusses the optical properties of these films. Among the various LbL-techniques that have been developed in the past[16], we focus on the popular spin-assisted LbL deposition technique[17] for the fabrication of thin-film nanocomposites. We provide detailed instructions on its use to fabricate composites of gold nanoparticle and polyelectrolyte multilayers.

In the second part of this article, we discuss the behavior of the LSPs that determine the optical properties of these nanocomposites. By evaluating the LSP resonance position by employing the MGEM theory, we show that the dielectric function of gold nanoparticles differs from the values for bulk gold. Moreover, we discuss films for which the environment cannot be approximated as homogenous material. The spatial range of the LSP is analyzed by successively covering the nanoparticles with polyelectrolyte layers. We then present an analytical procedure that allows us to approximate the spectral position of the LSP resonance for particles that are either partly sunken into a polymer

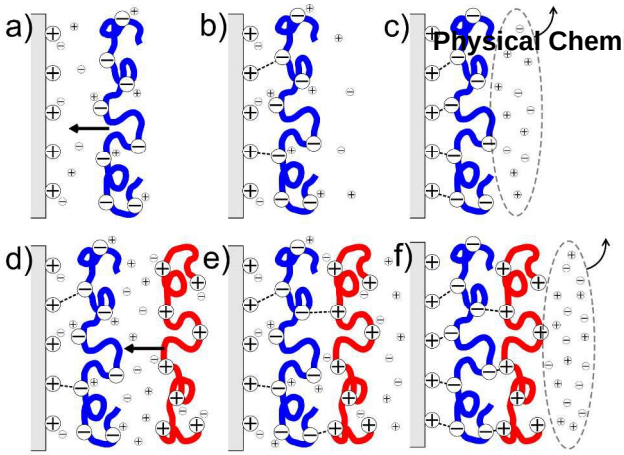

matrix or covered by thin polymer films. Finally, we compare the different behavior of the LSP depending on weather the metal

Scheme 1: Schematic illustration of layer-by-layer deposition. A negative charged polyelectrolyte (e.g. PSS) binds to a positive charged surface (a, b). Due to washing, the remaining counterions (Na+, Cl-) are removed and additional bonds are formed (c). In ionic solution, some bonds break up (d) and a positive charged polyelectrolyte (e.g. PAH) can adsorb (e). After washing and reformation of bonds (f) the process can be continued with the first step.

inclusion are gold nano-spheres (GNS) or gold nano-rods (GNR). The analysis is based on a thorough experimental characterization of the dielectric function of the polyelectrolytes by ellipsometry, the shape of the particles by scanning electron microscopy (SEM) and the embedding of the particles atomic force microscopy (AFM).

Assembly of Colloid-Polyelectrolyte Nanocomposites

From its invention LbL-deposition was closely related to colloidal nanoparticles. It was originally introduced by Iler et al., who used it for assembling multilayers of charged colloidal particles in the 1960s[18]. Subsequently, the method was extended to include single molecules and polyelectrolytes in the following years[19,20,22,33]. In this section we discuss the fabrication details of gold/polymer nanocomposites materials. It is intended to give the reader a "cooking recipe" for the layer-by-layer assembly of polyelectrolyte multilayers and gold nanoparticles.

Principles of Polyelectrolyte Layer-by-Layer Deposition

Polyelectrolytes combine the structure of a polymer with the electrostatic properties of an electrolyte. They consist of a linear or cross-linked backbone and charged side chains. In the dissolved state the side-chains are neutralized by Na^+ and Cl^- counter-ions (extrinsic charge compensation). In the presence of an additional oppositely charged polymer-surface, charge compensation by polymer-polymer bonding (intrinsic charge compensation) competes with the extrinsic compensation by counter-ions (Scheme 1 a-c). In order to increase the total system entropy, the intrinsic bonding releases the small ions that were electrostatically bound to the polymer. Intrinsic compensation is preferred and the polymer fully adsorbs to the surface. The resulting double-layer (DL) is electrically neutral.

To adsorb additional layers, polyelectrolyte layer overcompensation is necessary (Scheme 1 d-f). Adding additional NaCl to the solution shifts the equilibrium somewhat to extrinsic bonding. The additional Na^+ and Cl^- ions break up a part of the polyanion-polycation bonds, which results in a swelling of the film[14]. The unbound side chains provide the excess surface charge required for the adsorption of the next layer. Rinsing the completed sample with pure water releases the remaining ions and leads to the formation of a firm multi-layer system.

As each adsorption step comes along with a swelling of the film and a rearrangement of the polymer chains, very smooth film surfaces can be obtained and a pronounced self-healing effect of layer defects was observed[16].

Different fabrication methods implementing LbL exist[16,17,34,35]. The most common are: dip-coating[34], spray-coating[36] or spin-assisted[17] LbL deposition. The physical process described before is the identical for all three methods. However, from a technological perspective they have different advantages and disadvantages. As process for surface treatment, dip- and spray-coating are most suitable for objects with arbitrary shaped, non-planar surfaces. For applications on flat surfaces, spin-assisted LbL is much faster than dip- or spray coating. Moreover, it only needs a very low amount of solution. The layer properties depend on the fabrication method, since parameters as concentration and immersion time vary[35,37].

The thickness of one DL, consisting of two oppositely charged polyelectrolytes, is in the range of a few nanometers. Thus, these structures are applicable to build multilayers with a precisely tunable thickness. In principle, there is no limit to the layer number. We fabricated samples of several hundred DLs and multilayer systems of more than 1000 layers were reported[21].

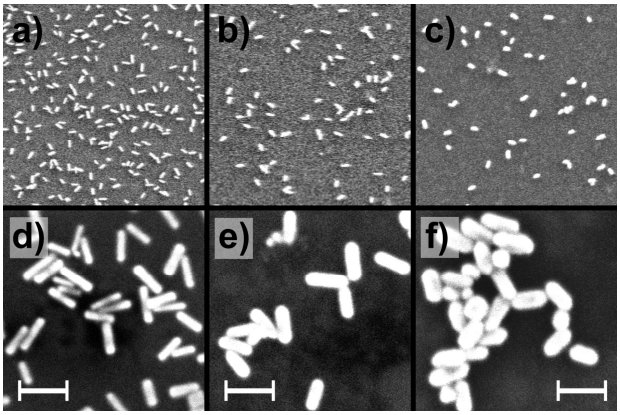

Figure 1: SEM pictures of the used GNRs type 1 (a, d), 2 (b, e), and 3 (c, f). The upper panel shows the in-plane distribution of the spectroscopic analyzed samples on an area of 2x2 µm². Below are high resolution pictures on Si substrates for size determination given in Table 1. The white bars represent 100 nm.

Fabrication of Gold Nano-Rods and -Spheres

NANO-SPHERES: Spherical gold nano-spheres (GNS), useful for LbL, can be produced by the wet-chemical reduction of *hydrogen tetrachloroaurate* ($HAuCl_4 \cdot 3H2O$) with *trisodium* citrate[38]. A solution of $HAuCl_4$ (c = 0.005 wt.) is heated to the boiling point. When citrate solution is added under continuous stirring, the color of the mixture turns to blue, indicating a nucleation of gold atoms. After several minutes, mono-dispersed particles form, while the color of the solution turns to dark red. The

particle size depends on the amount of the sodium citrate. In general, a higher citrate concentration yields a smaller particle size[39,40]. This procedure was first proposed by Hauser and Lynn in 1940[38] and realized some years later by Turkevich et al.[41] With slight modifications, it is still in use. Nowadays, commercial suppliers (e.g. Sigma-Aldrich) produce good quality GNS that can be used as received.

GNSs fabricated with this procedure have a negatively charged shell of citrate, so they adsorb to positively charged layers of PEI or PAH. If their adsorption to the polymer is weak, the addition of diluted HCl solution may help. Decreasing the pH value causes the protonation of NH_2-groups of the PAH. This in turn enhances the electrostatic attraction between these groups of the PAH and the COOH-group of the citrate particle shell.

NANO-RODS: For the preparation of Gold Nano-Rods (GNRs), separate seed and growth solutions are necessary. The seed solution consists of a mixture of aqueous $HAuCl_4$ solution (0.1 M, 0.75 mL) and *cetyl-trimethylammonium-bromide* (CTAB) (0.1 M, 9.75 mL) to which ice-cold aqueous $NaBH_4$-solution (0.01 M, 0.6 mL) is added. The growth solution is a mixture of aqueous solutions of $HAuCl_4$ (0.01 M, 2 mL), $AgNO_3$ (0.01 M, 0.4 mL), and CTAB (0.1 M, 40 mL) to which ascorbic acid (0.1 M, 0.32 mL) and HCl (1.0 M, 0.8 mL) are added sequentially. After the seed and growth solutions are mixed together the particles grow within several hours. More details of this recipe for the fabrication of GNRs were published by Yang et al. [42].

It should be noted, that only CTAB solutions from certain suppliers yield good results for the synthesis. This was examined by Smith et al., who found indications that a contamination of the CTAB with iodine is necessary for the successful growth of GNRs[43].

The optical properties of GNRs are related to their aspect ratio[10,44]. To tune the latter, glutathione can be selectively bound to the ends of the GNRs[42]. When exposed to the growth solution, the particle thickness increases whereas the glutathione prevents the growth in the length direction.

GNRs fabricated as described here are stabilized by a shell of CTAB molecules. Since CTAB is an amphiphilic molecule, these particles are difficult to incorporate into LbL films. Their applicability for LbL can be increased by coating the particles with one monolayer of PSS prior to the deposition. To do so, a solution of PSS (0.2% wt, 0.01 M NaCl) has to be added dropwise to the GNR solution under continuous stirring. The coated GNRs are separated from the remaining CTAB and PSS by double centrifugation of the solution. The PSS-coated particles are negatively charged and adsorb to layers of PEI or PAH.

Figure 1 shows SEM pictures of three types of GNR with different aspect ratios fabricated in our laboratories. Figure 2 display the size distribution evaluated from the SEM images in Figure 1 for all three rod types. Clearly, the distribution becomes broader for particles with a higher aspect ratio $R = A/B$. Table 1 summarizes the average particle length and diameter as well as the aspect ratio.

Because the interaction between metal-particles changes their electrical behavior, preventing particle clusters is crucial in order to obtain nanocomposites with controllable optical properties. Nanocomposites are thus best fabricated with low packing densities of the incorporated particles.

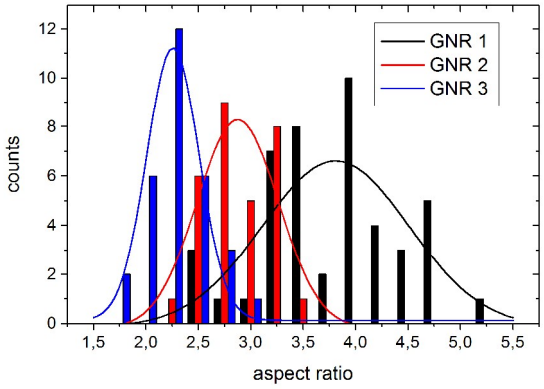

Figure 2: Distribution of aspect-ratio of GNR extracted from the SEM images in Figure 1. In particular GNR type 1 particles have a very broad size distribution.

Spin-Assisted Layer-by-Layer Deposition

Spin-assisted layer-by-layer deposition is the fastest method to produce polyelectrolyte multilayers on a flat sample. Here we describe the fabrication of PSS/PAH multilayer films, incorporating different types of gold nanoparticles by spin assisted LbL.

For optical experiments, fused silica discs (e.g. Ted Pella Inc.) with 1 inch diameter are ideal substrates for the nanocomposites. The substrates are cleaned by immersion in *peroxymonosulfuric*acid ("piranha solution": 50% H_2O_2, 50% H_2SO_4, **warning**: mixture will become hot and is a strongly oxidizing acid) prior to their use. After 30 minutes, it is rinsed with purified water and dried in nitrogen air flow. On one hand, this treatment removes organic remains from the substrate. More importantly, the strong acid adds OH groups and negative

Particle Type	Length /nm (A)	Diameter /nm (B)	AFM height /nm	Aspect Ratio (R)	Shape factor (u)	
					longitudinal	transversal
GNS 20	-	20 ± 2	-	1	2	-
GNR 1	62.5 ± 8.1	16.1 ± 1.5	13.4 ± 1.5	3.9 ± 0.6	11.93 ± 2.42	1.17 ± 0.01
GNR 2	70.1 ± 7.7	23.4 ± 2.8	19.4 ± 2.3	3.0 ± 0.3	8.27 ± 1.19	1.14 ± 0.01
GNR 3	79.0 ± 9.8	32.7 ± 2.7	30.4 ± 1.2	2.4 ± 0.3	6.15 ± 0.95	1.33 ± 0.01

Table 1: Size parameters and wavelengths of resonant absorption for GNSs and GNRs

charges to the substrate surface, which aid the bonding of the first polyelectrolyte layer.

During the layer depositions, the sample rotates at 3000 rpm. To provide a homogeneous surface charge, the clean substrate is initially wetted with solution of PEI (Poly(ethyleneimine), M_w ~750,000, e.g. Sigma-Aldrich;c=1% wt). A complete wetting of the substrate with PEI solution indicates a hydrophilic surface. To avoid drying the remains are washed away immediately by rinsing the sample with 3 drops of purified water. This washing ensures that only one monolayer of the polyelectrolyte is adsorbed. The subsequent layer (PSS) is deposited only after the layer is dried.

In order to form polyelectrolyte multilayers, PSS (Poly(sodium 4-styrenesulfonate), M_w ~70,000, e.g. Sigma-Aldrich) and PAH (poly(allylamine hydrochloride), M_w ~58,000, e.g. Sigma-Aldrich) layers are alternatingly deposited, in the same manner as described for PEI. It is important that the aqueous PSS and PAH solutions (c = 0.1% wt.) contain NaCl with a concentration of 1 mol/l, to guarantee charge overcompensation. Now the washing step is even more crucial, as it additionally prevents the crystallization of NaCl. Depending on humidity and temperature, a double-layer of PSS/PAH (DL) can be assembled every 60 seconds. Speeding up the preparation by skipping the drying step leads to a very rough film surface, due to the formation of aggregates of PSS and PAH.

We determined the thickness for one double-layer PSS/PAH by AFM, ellipsometry, and X-ray reflectivity measurements to be around 2.5 nm. The dielectric function of such a film, as determined by ellipsometry, is plotted in Figure 5a.

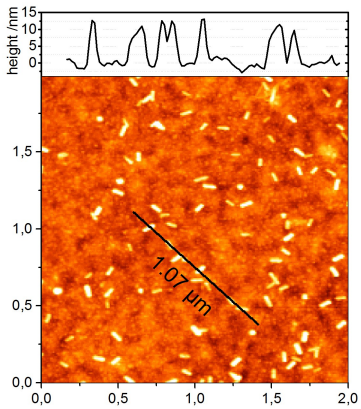

Figure 3: AFM pictures of GNR type 1 on 2x2 µm². The upper panel shows the topographic cross section along the black line.

To incorporate gold nanoparticles into the polymer matrix, a layer of PSS is simply replaced by a layer of particles. However, the low concentration of the GNS suspension and the weak surface charges of the particles complicate a spin-assisted deposition. Therefore, a technique similar to dip-coating has to be applied. The spin-coater is halted and the sample is completely covered with GNS suspension. Depending on the surface charge of the particles and the desired packing density, the adsorbing process lasts from several tens of minutes up to hours. The total immersion time, together with the concentration of the suspension, determines the in-plane packing density of the final film[16]. Due to their cover with PSS, the GNRs adsorb much faster. A spin-assisted deposition is possible, but the packing density increases with additional immersion time.

Figure 3 shows a typical AFM topography measurement of spin-casted GNR type 1 adsorbed on PAH with a total immersion time of 30 min. The effective height of the GNRs type 1 was around 10 nm, indicating that the particles were sunk 6 nm into the underlying polymer. Similarly, GNRs type 2 and 3 had a sinking depth of 5 nm and 3 nm, respectively, while the GNSs had a sinking depth of 2 nm. The particle density in all cases was approximately 30 particles per µm².

Maxwell-Garnett Effective Medium Theory

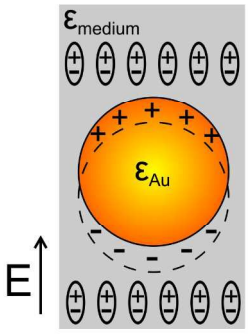

Scheme 2: Displacement of electrons due to an external field. For particles that are smaller than the wavelength, the field can be assumed as homogeneous.

The particular optical characteristics of nanoparticle composites originate from the collective oscillation of the particles' valence electrons, the localized surface plasmon (LSP)[10,11]. The electromagnetic field of a light-wave impinging on a metal nanoparticle displaces the quasi-free electrons and generates charged regions at the surface of the formerly neutral particle. If the particle dimension is smaller than the wavelength of light inside the particle material (< 100 nm for visible light), all electrons are deflected into the same direction. The Coulomb-forces between the oppositely charged surfaces present an effective restoring force and, consequently, an oscillating dipole is formed. The resonance condition for the dipole, or LSP resonance, is given if the macroscopic oscillating polarization of the dipole is in resonance with the incoming light. This resonance condition can be expressed in terms of the dielectric function, ε, of the particle, which presents a measure for its polarizability. The mathematical expression for the resonance condition depends on the precise geometry[10] and will be discussed later in this article.

Additionally, the electric field of the displaced charges on the metal particle polarizes the medium surrounding the particle (Scheme 2), which in turn modifies the restoring forces of the LSP dipole. The position of the LSP resonance is therefore determined not only by the dielectric function of the particle but also by the dielectric function of the environment. As a result, the LSP resonance frequency undergoes a bathochromic shift if the dielectric-function of the environment increases. This sensi-

tivity to subtle changes of the environment is a technologically very interesting property, e.g. for the use in highly sensitive sensors on a single molecule level [24–27].

The optical properties of a single nano-sphere, including the LSP resonance, can be calculated analytically by Gustav Mie`s theory for spherical colloids[43,45]. Predicting the properties of nanocomposites is more difficult, as both the dielectric functions of the matrix, ε_m, and of the inclusions, ε_{inc}, as well as the distribution of particles have to be taken into account. In this context effective-medium theories try to describe optical properties of the composite material by a single complex dielectric function, ε_{eff}, or complex index of refraction $\tilde{n}_{eff} = n_{eff} + i \cdot \kappa_{eff}$ [10,11,29,46]. In the following we describe how to employ the Maxwell-Garnet effective medium (MGEM) theory to nanocomposites including spherical or rod-like colloids and what information about the particle environment can be extracted from it.

We note that these considerations are strictly valid only for small particles (≤ 100nm). For larger particles additional multipole contributions and retardation effects must be taken into account[10].

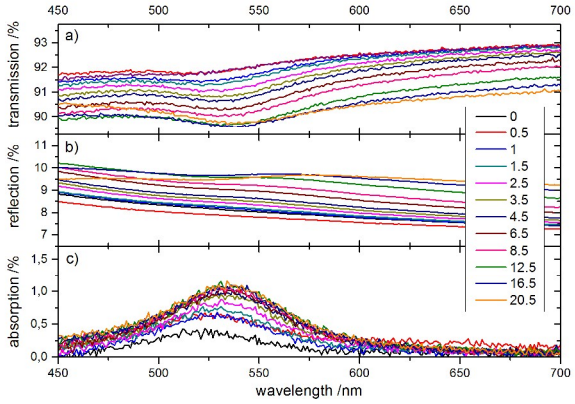

Figure 4: Series of transmission (a), reflection (b), and absorption (c) spectra for GNSs with 20 nm diameter. The arrows indicate the spectral changes while successive covering of the particles with double-layers (DL) of PSS/PAH.

MGEM for Nano-spheres:

A considerable number of effective-medium theories exist in literature, taking into account different geometries of the particles and the compositions of the material[10,29,30]. The MGEM describes the dielectric function of composite materials with sub-wavelength spherical inclusions in an embedding homogeneous medium. It uses a formula similar to the Clausius-Mossotti relation to calculate the effective dielectric function ε_{eff} of a medium containing diluted particles with a volume filling factor f:

$$\varepsilon_{eff} = \varepsilon_m + 3f \cdot \varepsilon_m \cdot \frac{\varepsilon_{inc} - \varepsilon_m}{\varepsilon_{inc} + 2\varepsilon_m} \qquad 1)$$

This formula was originally developed for small filling factors *($f < 0.01$)*. However experimental studies proved that the errors in the description of high filling factor composites by MGEM are minimal[10,47].

In the case of the ultrathin nanocomposites discussed in the first section of this article, $\varepsilon_{inc} = \varepsilon_{Au}$ for the GNS and $\varepsilon_m = \varepsilon_{poly}$ for the PAH/PSS polyelectrolyte matrix. The resonance condition for the LSP occurs if real part of the denominator in equation 1 vanishes *($\varepsilon_{Au} = -2\varepsilon_m$)*, giving rise to a local maximum of the real and imaginary part of ε_{eff}. The imaginary component of the dielectric function keeps ε_{eff} finite, because it prevents the resonance denominator from approaching zero. The factor 2 in the denominator of equation 1 describes the geometrical form of the spherical particles. Due to their spherical symmetry only one dipole LSP resonance occurs for GNS. For non-spherical particles on the other hand the geometrical factor has to be replaced by a more complex expression, which gives rise to more than one LSP[10,44].

Figure 4 presents typical transmission *T(λ)* (Figure 4a) and reflection spectra *R(λ)* (Figure 4b) of a nanocomposite containing particles with 20 nm diameter and a filling factor of 0.025, as well as the absorption spectra *A(λ)* calculated from this data (Figure 4c). The spectra show samples with an increasing number of polyelectrolyte double-layers on top of the particles. For uncovered GNS the LSP resonance occurs at 521 nm, while fully embedded particles have their absorption maximum at 534 nm.

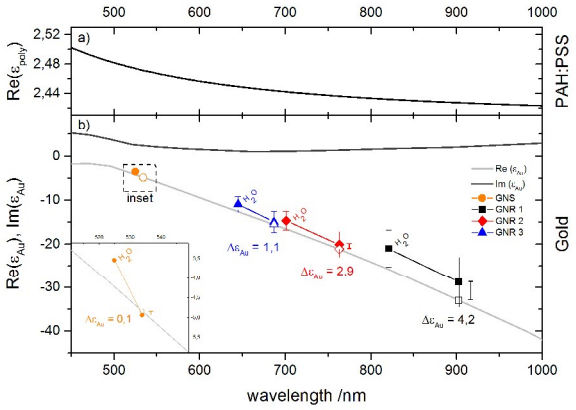

Figure 5: Plot of the dielectric function of PSS/PAH multilayers, ε_{poly}, (upper graph) and bulk-gold, $\varepsilon_{Au,bulk}$, measured by Johnson and Christy[48] (lower graph, grey lines). The values for ε_{Au} inferred from the LSP resonance wavelength and ε_{poly} by MGEM (lines & closed symbols) considerably differ from $\varepsilon_{Au,\ bulk}$ (open symbols) for all types of particles. The symbols marked with H_2O correspond to measurements of particles dispersed in distilled water. Error bars illustrate the uncertainties introduced by the measured size of the GNR via the shape factor G_A.

In the latter case, by evaluating the zero point of the denominator in equation 1, one can determine either ε_m, ε_{inc}, or the LSP resonance wavelength, λ_c, if each of the other two values is known. Figure 5 shows the real and imaginary part of $\varepsilon_{Au,\ bulk}$ as published by Johnson & Christy[48] (Figure 5b), as well as the real part of ε_{poly} for 50 double-layers of PSS/PAH measured by ellipsometry (Figure 5a). The open circle in Figure 5 (see also the inset of Figure 5) represents the value for $\varepsilon_{Au,\ bulk} = 2 \cdot \varepsilon_m$ in the case of fully embedded GNS as predicted from the measured λ_c and $\varepsilon_{Au,bulk}$. The value of $\varepsilon_m = 2.42$ obtained this way differs by approximately 2% from the value for the polymer matrix directly measured by ellipsometry of $\varepsilon_{ploy} = 2.47$. This

discrepancy is not caused by measurement uncertainties, but by the inaccurate use of $\varepsilon_{Au,bulk}$ in the calculation. Since the interatomic distance at surfaces is larger than in the bulk, the density of free electrons at surfaces is lower than in the bulk of the material. Small particles mainly consist of surface atoms. Consequently, their overall reduced electron concentration slightly shifts ε_{GNS} towards zero compared to $\varepsilon_{Au,bulk}$. Therefore, we tool the ellipsometric values and ε_{ploy} the measured λ_c to determine the modified dielectric function of nanoparticles ε_{GNS}. As a cross-check we determined ε_{GNS} at a second wavelength, by measuring the resonance of the same GNSs in distilled water ($\varepsilon_{aqu} = 1.78$)[49]. With about 18%, the discrepancy between $\varepsilon_{Au,bulk}$ and the measured ε_{GNS} is even more pronounced in this case. As the dielectric function of gold is almost linear between both measured wavelengths, we used a linear interpolation (orange lines in Figure 5) between these values as new $\varepsilon_{GNS}(\lambda)$. The large deviation of the resulting ε_{GNS} from $\varepsilon_{Au,bulk}$ towards lower wavelength, ultimately confirms that the observed difference between both cannot be caused by simple measurement uncertainties.

MGEM for Nano-rods:

Equation 1 is valid only for spherical particles. For spheroidal (i.e. rod-shaped) particles, the spherical symmetry is lifted in the spatial direction of its *major* (or *long*) axes. As a result the LSPR splits into two distinct resonances correlated to the major (longitudinal LSP) and minor (transverse LSP) axes. In this case, the shape factor 2 in the denominator of equation 1 has to be replaced by a more complex expression u_i that differs for each of the principal axes $i = A, B, C$. The LSP occurs, when the condition [10,44],

$$\varepsilon_{Au} = -u_i \cdot \varepsilon_m = -\frac{1-G_i}{G_i} \cdot \varepsilon_m \qquad (2)$$

is fulfilled. The geometrical factors G_i take into account the different geometries of the particle along its principle axis. A separate LSPR might occur for each principle axis (see sketches in Figure 6c). Nano-rods can be approximated as *prolate spheroids*, for which the two transverse axes (B, C) are identical while the longitudinal axis (A) is elongated with respect to the others. In this case, the geometrical factors are[10,34]:

$$G_A = \frac{1-e^2}{e^2}\left[\frac{1}{2e} ln\left(\frac{1+e}{1-e}\right) - 1\right] \qquad (3a)$$

$$G_B = G_C = \frac{1-G_A}{2} \qquad (3b)$$

Here $e = \sqrt{1 - 1/r^2}$ it the eccentricity of the spheroid, while r is the aspect-ratio of the major *(A)* towards the minor axes *(B, C)*. GNR spectra have two LSPs as the transverse resonances corresponding to the B and C axis are degenerate, while the longitudinal resonance, corresponding to the A axis, is shifted to lower energies. The LSPs of single GNRs are polarized along its major and minor axis, respectively. However, in most practical nanocomposites the rods are oriented statistically and both resonances are observed independently from the polarization of the incident light.

Figure 6 reproduces the measured transmission $T(\lambda)$ (Figure 6a), reflection $R(\lambda)$ (Figure 6b) and the calculated absorption $A(\lambda)$ spectra (Figure 6c) of GNRs with an aspect ratio of $r = 3.9$ (type 1). Without polymer cover, two resonances occurred, corresponding to the longitudinal (783 nm) and transverse (511 nm) LSP resonances. The resonances of the covered particles shifted bathochromically to 893 nm and 514 nm, respectively.

Again, the values (open symbols) for ε_m extracted by MGEM from the measured λ_c and $\varepsilon_{Au,bulk}$ (Johnson and Christy) differ considerably (up to 15%) from the values for ε_{poly} directly measured by ellipsometry. We therefore determined a corrected ε_{GNR} using the same procedure described for GNS. Figure 5 shows the corrected ε_{GNR} for all three types of rods. Interestingly, the deviation of ε_{GNR} from $\varepsilon_{Au,bulk}$ depends on the size of the rod. For larger particles, ε_{GNR} strives towards $\varepsilon_{Au,bulk}$. This observation affirms the interpretation of lower electron densities for small gold nanoparticles as source of the modification of ε_{Au} in this case.

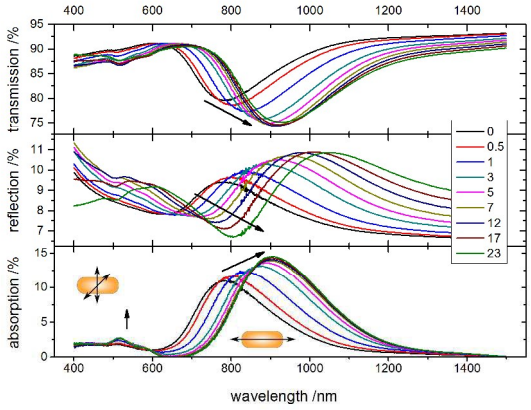

Figure 6: Series of transmission (a), reflection (b), and calculated absorption (c) spectra for GNR type 1. The arrows indicate the spectral changes due to covering the particles with double-layers (DL) of PSS/PAH. The pictures in (c) illustrate the transverse plasmon absorption at ~520 nm and the longitudinal one in near infrared.

Spatial Range of Localized Surface Plasmons

Covering nanoparticles by polyelectrolyte DLs, shifts the resonances to longer wavelength (indicated by the arrows in Figure 4 and Figure 6). With increasing cover layer thicknesses the effective epsilon of the environment, ε_{env}, increases from the value for air $\varepsilon_{air} = 1$ to the value for the polymer $\varepsilon_{poly} = 2.47$. The change in ε_{env} subsequently causes a red-shift of the LSP resonance. As LbL allows the deposition of very homogenous layers, the resonance layer shift versus the cover layer thickness can be used to determine the effective range of the LSP excitation. The intensity of the LSP near-field decays with $1/r^6$ [10,11]. The environment in close vicinity to the particle is therefore more strongly polarized by the LSP than the wider environment. Therefore, each successive layer deposited onto the particles influences the LSP of the particle less. Finally, changes of the dielectric environment far away from the particle do not

influence the LSP absorption and the modification of the LSP resonance saturates for large cover thicknesses. Thus, measuring the saturation allows us to determine an effective range of the LSP excitation.

The samples used in Figure 4 and Figure 6 were structured according to the layer sequence $[(PSS/PAH)_8Au(PAH/PSS)_n]$, where n is the number of DLs. The total cover layer thickness is hence $d_n = n \cdot d_{DL}$, with an average DL thickness of $d_{DL} = 2.5nm$ as mentioned above. The structure of the nanocomposites was identical for spherical (Figure 4) and rod-like (Figure 6) inclusions. All optical spectra were obtained as follows: We collected the transmission $T(\lambda)$ and the reflection spectrum $R(\lambda)$ using a spectrometer equipped with an Ulbricht sphere (Agilent Technologies Cary 5000) and subsequently calculated the absorption by $A(\lambda) = 1 - T(\lambda) - R(\lambda)$. $T(\lambda)$ was measured at normal incidence and $R(\lambda)$ at an angle of 3° 20'. Moreover, both spectra were corrected for the weak diffuse scattering (< 1 %) of the particles.

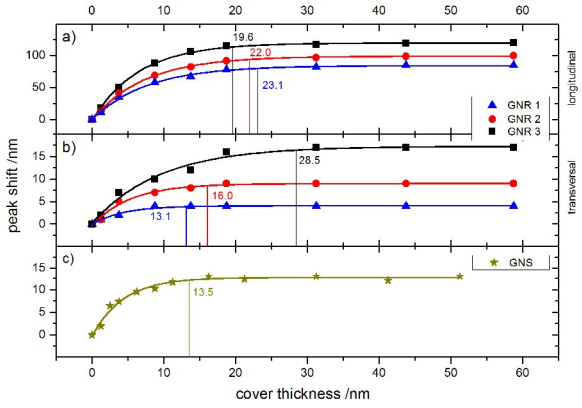

Figure 7: Shift of plasmon resonance depending on cover layer thickness. The lines are polynomial fits according to $(A-B/r^6)$, where r is the cover layer thickness, A is the saturation asymptote and B is an arbitrary fitting parameter. The marked values of layer thickness correspond to 95% of saturation parameter A. The longitudinal LSPs (a) saturate for different values than the transverse LSP (b) of the GNRs. The LSP of the GNS (c) saturates at a similar value as the transverse LSP of the smallest GNR, which has a width comparable to the size of the GNS.

For the discussion of the influence of the dielectric matrix on the LSP resonance, we extracted the resonance shift $\Delta\lambda$ from the absorption spectra by a Gaussian fit to the respective plasmon absorption bands. In the case of GNRs, transverse and longitudinal peaks were evaluated separately.

GOLD NANO-SPHERES: Figure 7c presents $\Delta\lambda$ versus the cover thickness d_n for GNSs with 20 nm diameter. At low d_n $\Delta\lambda$ increased rapidly with increasing d_n. On the other hand, at high d_n both parameters converged towards a saturation value. The thickness, at which the transition between both behaviors occurs, corresponds to the effective range of the LSP. We evaluated the transition point d_{sat} by fitting the data points with a generic sixth order polynomic function $(A-B/r^6)$ corresponding to the decay of the electric near-field intensity of the particle. Here, A is a saturation asymptote and B is an arbitrary fitting parameter. The saturation thicknesses were chosen at the position where $\Delta\lambda$ reaches 95% of the upper bound A. The results are presented in Figure 7.

GOLD NANO-RODS: In the case of GNRs, one has to distinguish between transverse (minor particle axis) and longitudinal (major axis) LSP resonances. Figure 7b shows the evaluation of $\Delta\lambda$ versus d_n for the transverse LSP of GNRs with three different aspect ratios. Figure 7a depicts the evaluation of the corresponding longitudinal LSP. Qualitatively, both LSPs showed the same saturation behavior we reported for GNSs. Quantitatively the total shift $\Delta\lambda_{tot}$ between the uncovered and the fully covered GNRs was much more pronounced for the longitudinal LSPs (85 – 110 nm) than for the transverse LSPs (3 – 17 nm). The transverse LSP shift moreover approximately matched $\Delta\lambda$ observed for the GNS and saturated for a cover thickness comparable to the particles diameter. The more pronounced longitudinal LSP shift on the other hand saturated around 20 nm, irrespective of the precise particle dimensions.

Effective Dielectric Function of Nanocomposites with a Two-Phase Matrix

The Maxwell-Garnett theory describes the LSP of a dispersion of nanoparticles in a homogeneous dielectric medium[30]. If, however, the medium surrounding the particles is thinner than the LSP interaction distance, d_{sat}, as introduced in the last section, we cannot speak any longer of a homogeneous medium, as the polyelectrolyte matrix does not fully screen the particle from the wider environment (i.e. air). The correct LSP behavior in this case could be determined by extensive numerical calculations using finite-elements or distribute-dipole approaches [14,15,31,32].

Here we follow a simpler approach. We show that the LSP resonance wavelength can be calculated using MGEM, if one assumes that the two-phase medium surrounding the particles forms a homogeneous environment with an effective ε_m between ε_{poly} and ε_{air}[23].

As noted earlier in this article, the polarization of the environment by the LSP reacts back on the LSP itself and shifts the resonance frequency. In the case of heterogeneous media, polarizations of different media contribute to the effective over-all polarization of the environment. In the linear optical regime, thus for low light intensities, the fields caused by the polarization of the different materials simply add up. We therefore estimated ε_m by calculating a weighted average of the dielectric functions ε_{poly} and ε_{env}, according to:

$$\varepsilon_m = x \cdot \varepsilon_{poly} + (1 - x)\varepsilon_{air} \qquad (4)$$

The weighting factor, x, reflects the relative influence of the polyelectrolyte on the LSP resonance. From a physical point of view, an LSP is characterized by an electrical near-field originating at the nanoparticle surface and decaying into the material on both sides. The (induced) polarization of the surrounding medium, given by the dielectric function, modifies the electric field strength and therefore the LSP resonance wavelength.

If the electric near-field of the particle is known, the relative influence of the two phases can be determined by calculating

the volume integral over the electrical near-field intensity of the LSP:

$$V' = \int I \, dV = \int E^2 \, dV \qquad (5)$$

For GNS and GNR established analytical solutions for the electric field exist[10] and the calculation of equation (5) is straight forward.

The weighting factor is subsequently given by the ratio of the near-field weighted polyelectrolyte volume, V'_{poly}, to the total near-field weighted volume (polyelectrolyte plus air), V'_{tot}, around the particle:

$$x = \frac{V'_{poly}}{V'_{tot}} \qquad (6)$$

With this simple approach we were able to accurately reproduce the central wavelength of the LSP for different film thicknesses.

Although we could find an approximate analytical solution of the problem yielding the same result, we show the results of numerical integration of equation (5). We calculated the effective dielectric function of the environment of partly covered GNS and GNR. The integral in (5) has to be evaluated in principle from the particle-surface to infinity. We limited the numerical evaluation to an upper bound corresponding to d_{sat}. Calculations for slightly greater volumes showed that the weighting factor did not change anymore beyond this point. All input parameters are either listed in or can be calculated from the values in table 1.

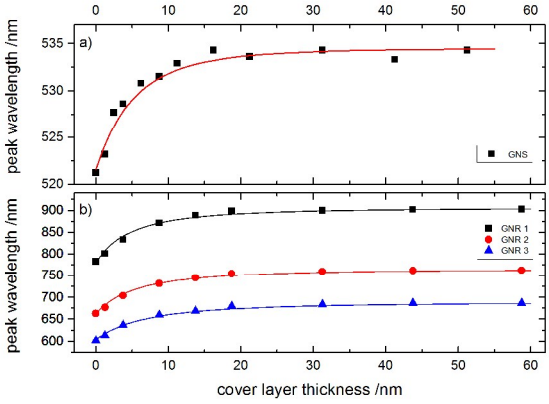

Figure 8: The peak-shift calculated for 20nm-GNSs (a, line) and for all three types of GNRs (b, lines) corresponds very well to the measured shifts (a,b, symbols). The calculation assumes an adjusted real-part of ε_{Au} (Figure 5) inferred from the measured values for fully polymer-embedded GNS and for GNS emerged in distilled water.

Figure 8 shows the results of the calculation for GNSs and GNRs, respectively (straight lines). Indeed, using the corrected ε_{GNS} and ε_{GNR} (Figure 5b) and the measured ε_{poly} (Figure 5a), the calculated shift $\Delta\lambda$ reproduced the measurements very well. For an accurate fit of the initial wavelength, one has to take into account that also the uncovered particles are sunken into the material (see AFM measurements Figure 3 and table 1).

Conclusions

In conclusion, in this perspectives article we discussed the fabrication and optical properties of ultrathin gold-nanocomposite films. We described the preparation of nanocomposite samples, based on gold nano-spheres and nano-rods, by spin-assisted layer-by-layer as a low-cost, ultra-robust fabrication technique and discussed the advantages and pitfalls of this approach.

We confirmed that the dielectric function of gold nanoparticles differs from the dielectric function of bulk gold. Moreover, we demonstrated that the effective interaction range of nanoparticles can be determined by the successive covering of these particles with polyelectrolyte layers. The careful assessment of the nanostructures by various experimental techniques allowed us to verify the application of the Maxwell-Garnet effective medium theory to particles in a two-phase environment. By weighting the dielectric functions of both environment materials, polymer and air, with the near field intensity, we were able to accurately reproduce the observed plasmon shift.

The techniques for the preparation and investigation of nanocomposites discussed in this article are by no means limited to the materials and particles introduced here, but rather can be applied to all kinds of nanocomposite systems. The rapid and reproducible fabrication of such nanolayers may be easily transferred to other physico-chemical laboratories, where the self-consistent evaluation may be extended to many other nanoscale systems with exciting optical properties.

Acknowledgements

The authors want to express their gratitude to Carsten Henkel for the fruitful discussions about the theory of plasmon resonances in multiphase materials and to Andreas Hertwig of the Federal Institute for Materials Research and Testing for the ellipsometry measurement. We acknowledge the experimental support with AFM measurements by the group of Svetlana Santer and with SEM measurements by Frank Jaiser.

Notes and references

[a] Institut für Physik und Astronomie, University of Potsdam, 14476 Potsdam, Germany
[b] Helmholtz Zentrum Berlin, 12489 Berlin, Germany
*koopmann@uni-potsdam.de

References

1. L. Zhai, A. J. Nolte, R. E. Cohen and M. F. Rubner, *Macromolecules*, 2004, **37**(16), 6113.
2. L. Zhai, M. C. Berg, F. C. Cebeci, Y. Kim, J. M. Milwid, M. F. Rubner and R. E. Cohen, *Nano Lett.*, 2006, **6**(6), 1213.
3. J. Hiller, J. D. Mendelsohn and M. F. Rubner, *Nature Mat*, 2002, **1**(1), 59.
4. B. Thierry, F. M. Winnik, Y. Merhi, J. Silver and M. Tabrizian, *Biomacromolecules*, 2003, **4**(6), 1564.

5. C. M. Jewell, J. Zhang, N. J. Fredin, M. R. Wolff, T. A. Hacker and D. M. Lynn, *Biomacromolecules*, 2006, **7**(9), 2483.
6. X. Su, B.-S. Kim, S. R. Kim, P. T. Hammond and D. J. Irvine, *ACS Nano*, 2009, **3**(11), 3719.
7. K. C. Wood, H. F. Chuang, R. D. Batten, D. M. Lynn and P. T. Hammond, *Proc. Natl. Acad. Sci. U.S.A.*, 2006, **103**(27), 10207.
8. D. Kim, Y. Kim and J. Cho, *Chem. Mater.*, 2013, **25**(19), 3834.
9. S. Mallidi, T. Larson, J. Aaron, K. Sokolov and S. Emelianov, *Opt. Express*, 2007, **15**(11), 6583.
10. M. Quinten, *Optical Properties of Nanoparticle Systems: Mie and Beyond*, Wiley-VCH, Weinheim, 2011.
11. U. Kreibig and M. Vollmer, *Optical Properties of Metal Clusters*, Springer, Berlin, 2010.
12. A. E. Neeves and M. H. Birnboim, *J. Opt. Soc. Am. B*, 1989, **6**(4), 787.
13. E. Prodan, A. Lee and P. Nordlander, *Chemical Physics Letters*, 2002, **360**(3-4), 325.
14. W. A. Murray, B. Auguié and W. L. Barnes, *J. Phys. Chem. C*, 2009, **113**(13), 5120.
15. Y.-F. Chau and Z.-H. Jiang, *Plasmonics*, 2011, **6**(3), 581.
16. G. Decher in *Multilayer thin films: Sequential assembly of nanocomposite materials*, ed. G. Decher and J. B. Schlenoff, Wiley-VCH, Weinheim, op. 2003, p 1.
17. M. Kiel, S. Mitzscherling, W. Leitenberger, S. Santer, B. Tiersch, Sievers, T. K., H. Möhwald and M. Bargheer, *Langmuir*, 2010, **26**(23), 18499.
18. R. K. Iler, *Journal of Colloid and Interface Science*, 1966, **21**(6), 569.
19. de Villiers, Melgardt M, D. P. Otto, S. J. Strydom and Y. M. Lvov, *Advanced drug delivery reviews*, 2011, **63**(9), 701.
20. J. H. Fendler, *Chem. Mater.*, 1996, **8**(8), 1616.
21. K. M. Lenahan, Y.-X. Wang, Y. Liu, R. O. Claus, J. R. Heflin, D. Marciu and C. Figura, *Adv. Mat.*, 1998, **10**(11), 853.
22. J. Koetz and S. Kosmella, *Polyelectrolytes and nanoparticles: With 6 tables*, Springer, Berlin, Heidelberg, 2007.
23. M. Kiel, M. Klötzer, S. Mitzscherling and M. Bargheer, *Langmuir*, 2012, **28**(10), 4800.
24. P. V. Ruijgrok, P. Zijlstra, A. L. Tchebotareva and M. Orrit, *Nano Lett.*, 2012, **12**(2), 1063.
25. K. Yu, P. Zijlstra, J. E. Sader, Q.-H. Xu and M. Orrit, *Nano Lett.*, 2013, **13**(6), 2710.
26. V. Mankad, P. K. Jha and Ravindran, T. R., *J. Appl. Phys.*, 2013, **113**(7), 74303.
27. S. Kumar, M. Anija and A. K. Sood, *Plasmonics*, 2013, **8**(3), 1477.
28. J. C. M. Garnett, *Philosophical Transactions of the Royal Society A: Mathematical, Physical and Engineering Sciences*, 1904, **203**(359-371), 385.
29. D. E. Aspnes, *Am. J. Phys.*, 1982, **50**(8), 704.
30. G. A. Niklasson, C. G. Granqvist and O. Hunderi, *Applied Optics*, 1981, **20**(1), 26.
31. N. G. Khlebtsov, *Journal of Quantitative Spectroscopy and Radiative Transfer*, 2013, **123**, 184.
32. K. L. Kelly, E. Coronado, L. L. Zhao and G. C. Schatz, *J. Phys. Chem. B*, 2003, **107**(3), 668.
33. N. E. Cant, H.-L. Zhang, K. Critchley, T. A. Mykhalyk, G. R. Davies and S. D. Evans, *J. Phys. Chem. B*, 2003, **107**(49), 13557.
34. G. Decher, *Science*, 1997, **277**(5330), 1232.
35. E. V. Skorb and D. V. Andreeva, *Polym. Chem.*, 2013, **4**(18), 4834.
36. M. Lefort, F. Boulmedais, L. Jierry, E. Gonthier, J. C. Voegel, J. Hemmerlé, P. Lavalle, A. Ponche and P. Schaaf, *Langmuir*, 2011, **27**(8), 4653.
37. M. An and J.-D. Hong, *Thin Solid Films*, 2006, **500**(1-2), 74.
38. E. A. Hauser and J. E. Lynn, *Experiments in colloid chemistry*, McGraw-Hill Book Co, New York, London, 1940.
39. G. Frens, *Nature Physical Science*, 1973, **241**(105), 20.
40. K. C. Grabar, R. G. Freeman, M. B. Hommer and M. J. Natan, *Anal. Chem.*, 1995, **67**(4), 735.
41. J. Turkevich, P. C. Stevenson and J. Hillier, *J. Phys. Chem.*, 1953, **57**(7), 670.
42. Z. Yang, W. Ni, X. Kou, S. Zhang, Z. Sun, L.-D. Sun, J. Wang and C.-H. Yan, *J. Phys. Chem. C*, 2008, **112**(48), 18895.
43. D. K. Smith and B. A. Korgel, *Langmuir*, 2008, **24**(3), 644.
44. S. Link and M. a. El-Sayed, *J. Phys. Chem. B*, 1999, **103**(40), 8410.
45. J. D. Jackson, *Classical electrodynamics*, Wiley, New Delhi, 2012.
46. T. Ung, L. M. Liz-Marzán and P. Mulvaney, *Colloids and Surfaces A: Physicochemical and Engineering Aspects*, 2002, **202**(2-3), 119.
47. U. Kreibig, A. Althoff and H. Pressmann, *Surface Science*, 1981, **106**(1-3), 308.
48. P. B. Johnson and R. W. Christy, *Phys. Rev. B*, 1972, **6**(12), 4370.
49. W. M. Haynes and D. R. Lide, eds., *CRC handbook of chemistry and physics: A ready-reference book of chemical and physical data*, CRC Press, Boca Raton, Fla., 2013.